A study of drop-coated and chemical bath-deposited buffer layers for vapour phase deposition of large area, aligned, zinc oxide nanorod arrays

D. Byrne[1], E. McGlynn[1], M. Biswas[1], M.O. Henry[1], K. Kumar[2], G. Hughes[2]*

[1]School of Physical Sciences, National Centre for Plasma Science and Technology, Dublin City University, Glasnevin, Dublin 9, Ireland

[2]School of Physical Sciences, National Centre for Sensor Research, Dublin City University, Glasnevin, Dublin 9, Ireland

*Author to whom correspondence should be addressed: enda.mcglynn@dcu.ie

Abstract

Zinc oxide films derived from drop-coating solutions of zinc acetate in ethanol followed by chemical bath deposition were examined for their suitability as buffer layers for high temperature vapour phase deposition of large area, aligned, zinc oxide nanorod arrays. An XPS analysis of substrates drop coated with zinc acetate solutions clarifies the chemistry of the deposition mechanism of the initial acetate-derived ZnO seeds. SEM, AFM and white light profilometry studies show that while zinc acetate-derived buffer layers are suitable for chemical bath deposition of aligned zinc oxide nanorod arrays, during high temperature vapour phase depositions these buffer layers undergo substantial changes leading to a loss of nanorod alignment and poor substrate coverage. We present a method to deposit aligned zinc oxide nanorod arrays uniformly over large area substrates, which combines zinc acetate drop coating, chemical bath deposition of buffer layers and vapour phase transport deposition of nanorods.

1. Introduction

ZnO has attracted considerable attention in the last decade, as a potential material for optoelectronic and other device applications. Its wide direct bandgap of 3.3eV at 300K and exciton binding energy of ~60 meV[1] has fueled interest in this material for electronic and optoelectronic devices, such as field emitters, UV lasers/LEDs and photovoltaic cells[2-4] The surface reactivity of ZnO has also attracted interest for applications such as solid state gas sensors[5-6], while theoretical predictions suggest that transition metal doped ZnO may be ferromagnetic and suitable for room temperature spintronic applications.[7] Other novel ZnO applications have been developed, such as nano-electrical generators based on the piezoelectric properties of quasi 1D nanorod arrays.[8] ZnO also has other notable material advantages in that it is biocompatible[9], available in high purity at low cost and compatible with many aspects of conventional silicon processing technology.[2]

A wide variety of ZnO nanostructures has been developed, such as thin films, walls, rods, belts, springs and hemispheres.[10-16] Aligned ZnO nanorod arrays are an interesting subset of these morphologies. The large surface area of nanorod arrays makes them ideal for applications such as gas sensors, substantially increasing their sensitivity.[6] It has been shown that dense nanorod arrays can be used to increase dye loading in solar cells while maintaining efficient carrier collection, improving the performance of these cells.[12] ZnO nanorod arrays have been investigated for use as field emitters, where their high aspect ratio, good chemical and mechanical stability are expected to yield high current densities and stable performance.[17]

The range of techniques used to grow ZnO nanorod arrays is quite diverse, with techniques such as low temperature chemical bath depositions (CBD) of various types, hydrothermal deposition[12-13, 18-19] and higher temperature techniques such as vapour phase transport (VPT) and chemical vapour deposition.[20-21] CBD is of particular interest due to its low cost, ease of implementation on diverse substrates and scalability. In general, CBD relies on the reaction of a zinc salt with hydroxide species in solution to form a zinc hydroxide intermediate, which subsequently decomposes to form ZnO. Alternatively, depending on the reaction conditions, the reaction of Zn^{2+} ions with hydroxide ions forms

ZnO directly without the intermediate hydroxide.[22] The growth of ZnO nanorods via CBD is improved if the substrate has been pre-seeded with ZnO crystallites.[12-13, 19, 23-24] The presence of ZnO seeds on the substrate provides nucleation sites for the subsequent growth of the ZnO nanorods. Earlier work, utilising ZnO seeded substrates clearly showed the scalability of this technique, as samples the size of full silicon (Si) wafer slices were easily produced.[24] Despite the ease in implementing CBD techniques, the optical quality (as determined by bound exciton linewidths at low temperatures) of ZnO nanorods deposited in this manner is generally significantly poorer than nanorods grown by other techniques such as VPT.[25-26] In addition, CBD is a relatively slow technique, with deposition times up to 50 hours being reported.[12] During such long deposition times, to prevent nanorods agglomerating into a thin film, it is necessary to use surfactants to cap the lateral facets of the ZnO crystals.[12, 19, 27]

In contrast, vapour phase techniques such as carbothermal reduction VPT are relatively fast and clean, depositing higher optical quality nanorods, with reasonable lengths (1-3 μm) in growth times of approximately 1 hour. However, the factors affecting vapour phase deposition are more complex, which makes reproducible nanorod growth more difficult to achieve. This can be considered a critical factor if ZnO is to be incorporated into industrial applications in a scaleable manner. In order to deposit aligned ZnO nanorods using VPT growth methods it is generally necessary to use an epitaxially matched substrate in combination with a suitable catalyst such as copper or gold. More recently, ZnO pre-seeded substrates have been used to initiate growth, providing nucleation sites for ZnO nanorods. Seeded substrates have been prepared in a variety of ways including drop coating of Zn salt solutions, pulsed layer deposition, direct-current reactive magnetron sputtering and radio frequency magnetron sputtering.[28-29] Previous studies have shown that the VPT techniques are sensitive to the substrate temperature, the texture and thickness of the ZnO buffer layer.[13, 28-29] Despite the many factors affecting nanorod growth on ZnO buffer layers, this technique offers distinct advantages over traditional catalyst-based methods, in that, the range of substrates is not limited to those that are epitaxially matched to ZnO and the potential for unintentional doping of the nanorods by the catalyst is negated.

We now consider the issue of scalability. While excellent results, in terms of nanorod alignment and material quality, have been reported using buffer layers prepared in a variety ways, many of these techniques rely on complex equipment setups which would present significant challenges if they were to be incorporated into an industrial scale process. In contrast purely solution-based growth methods are significantly easier to scale up but lack the high material quality desired for advanced applications. Therefore, combining solution-based deposition to create ZnO buffer layers which act as nucleation sites for subsequent carbothermal reduction-based VPT deposition may be a promising technique to overcome the shortcomings in both CBD and VPT techniques. The scalability of solution-based methods facilitates the deposition of large area short nanorod arrays quickly on a wide variety of substrates, using facile equipment setups, which can then be used as buffer layers to deposit high material quality nanorod arrays using VPT techniques, maximising the potential for scaling up VPT growth systems by using large area (~1-2 cm^2) buffer layers. Despite the potential advantages in combining solution-derived buffer layers with VPT deposition, there have been few reports on this subject.[30-31]

The method developed by Greene *et. al.*, using solutions of zinc acetate in ethanol to generate thin ZnO seed layers for CBD, has become an invaluable tool, widely used by many research groups to initiate aligned ZnO nanorod growth in solution, and is compatible with a range of substrates, including non-crystalline ones, such as glass.[13] However uncertainty surrounds these seed layers, as conflicting reports as to their chemical origin and deposition mechanism exist.[13, 32] In this work we examine in detail the chemical origins and deposition mechanism of acetate-derived ZnO seed layers as this is a critical component in generating large area, well-aligned CBD nanorod arrays as buffer layers for VPT. We also examine the effect of using acetate-derived seed layers and thicker CBD-derived buffer layers on VPT deposition and present a method to deposit high quality ZnO nanorod arrays which is reproducible, easily implemented on diverse substrates (due to the compatability of the seeding and CBD steps) and potentially scalable for industrial applications.

2. Experimental

2.1 Seed layer preparation

Silicon (111) wafers were cleaved into rectangles typically 1-4 cm^2 in area, cleaned by sonication in acetone followed by ethanol and dried in a nitrogen stream. No attempt was made to remove the Si native oxide layer. A thin seed layer was deposited by drop coating 3.5 - 4 μL of a 0.005 molar zinc acetate in absolute ethanol solution per cm^2 of substrate. The ethanol solution was allowed to remain on the substrate surface for 20 seconds before being rinsed off with copious quantities of fresh ethanol and dried with a gentle stream of nitrogen. The drop coating procedure was repeated a further four times, after which the substrate was annealed at 350°C in air for 30 minutes. This process leaves a thin film of textured/aligned ZnO crystallites which act as nucleation sites during subsequent ZnO growth, as per the report of Greene *et. al.*.[13]

2.2 Chemical bath deposition

ZnO nanorods were deposited on acetate-derived seeds by two different CBD techniques. In the first, pre-seeded substrates were submerged in a 25mM equi-molar solution of zinc nitrate and hexamethyltetramine at room temperature. The solution was heated to 85-90°C and maintained at this temperature for 30 minutes, with gentle stirring. After this time the substrates were removed from the reaction solution, washed with DI-H_2O and dried with nitrogen. In the second technique, 20 ml of a 0.02 molar zinc nitrate solution was slowly added to 20 ml of a 0.8 molar NaOH solution with vigorous stirring. This mixture was heated to 70°C before pre-seeded substrates were submerged into the reaction solution mixture. The solution was maintained at 70°C with stirring for 25 minutes before the substrates were removed, washed with DI-H_2O and dried with nitrogen.

2.3 Carbothermal reduction VPT deposition

Equal masses (0.06 g) of ZnO and graphite were carefully mixed to create a homogenous powder, which was distributed evenly across a 2 cm length of an alumina boat. Pre-seeded substrates or substrates which had chemical bath-deposited nanorods were placed directly above the ZnO/graphite powder mixture resting on the side walls of the alumina boat or on thin Si supporting strips (depending on the substrate size) . The substrate and boat were loaded in to a horizontal single zone tube furnace fitted with a quartz tube (length: 1.15 m; inner diameter: 37 mm). The boat was then heated to 925°C with a 90 sccm flow of argon through the furnace. The boat was maintained at this temperature for 1 hour before being cooled to room temperature and removed.

2.4 Characterisation

The morphologies of the deposits were examined using scanning electron microscopy (SEM; Karl-Zeiss EVO series). Surface morphology was examined by atomic force microscopy (AFM; Veeco Nanoscope Dimension 3100) operating in tapping mode using aluminium-coated silicon AFM probes, with a resonant frequence of 300kHz. Surface profiles of samples were investigated using white light profilometry (WLP; Veeco Wyko NT1100). Material surface composition was studied using a Vacuum Generators X-ray photoelectron spectrometer (XPS) at base pressures in the preparation and analysis chambers of $2x10^{-6}$ and $1x10^{-9}$ mbar, respectively, using an Al Kα ($h\gamma$ =1486.6 eV) x-ray source. The pass energy of the analyser was set at 20 eV yielding a resolution of approximately 1.0 eV. The XPS peaks were fitted with mixed ratio of Gaussian and Lorentzian line shapes and a Shirley background function. The calibration of the binding energy scale was performed with the C1s line (285 eV) from the adventitious carbon contamination layer.[33]

3. Results and discussion

3.1 Chemical pathway for acetate-derived seeds

Originally it was reported that drop coating solutions of zinc acetate in ethanol resulted in a thin residual layer of zinc acetate remaining on substrate surface, which is subsequently decomposed during the 350°C annealing step.[13] Later reports suggested that this was not the case and that the origin of the seed layer was due to a more complex process whereby atmospheric water diffused into the alcoholic solution and hydrolysed the acetate, forming an insoluble zinc hydroxide precipitate which remains on the substrate surface.[32] As the initial buffer layer preparation is a critical factor in depositing well-aligned nanorod arrays in solution, it is important to identify the precise origin of the seed layer. To clarify the chemical pathway, XPS analysis was performed on substrates after drop-coating solutions of zinc acetate in ethanol prior to and after annealing. Coated substrates were annealed in air at 350°C and under vacuum in the XPS chamber at 300°C and 450°C respectively.

The C 1s region of the spectrum shows similar features for samples before and after annealing, including C-C (285 eV) and C=O (286.5 eV) contributions, as shown in figure 1. A slight variation is observed between the first unannealed substrate which has a HO-C=O (289.7 eV) peak, while the remainder of the samples have an O-C=O (289.1 eV) contribution. After annealing all the samples have a similar distribution of chemical environments. Little variation is observed in the C-C peak intensity before and after annealing, suggesting that this peak is primarily due to adventitious carbon and not due to the C-C bond from the acetate group. While residual acetate and its decomposition products may contribute to the carboxyl signals at 286.5 eV 289.7 eV and 289.1 eV, it is likely that parts of these signals are due to surface adsorbed carbonates and hydrogen carbonates. It well established that both CO and CO_2 are readily adsorbed onto the surface of ZnO.[34-36] Previous XPS analysis on thin film samples prepared directly from ZnO by sputtering, without the use of acetate salts, show similar peaks in this region, which were attributed to surface carbonates or hydrocarbonates.[37] While the higher binding energy peak position sheds little information as to the origin of the carbonates, some further insight can

be gained from the relative peak intensity. In figure 1 it can be seen that the higher binding energy contribution prior to annealing is small in comparison to dominant adventitious carbon peak, similar to the results obtained for acetate-free ZnO by Saw *et. al.*.[37] In direct decomposition studies of acetate salts (zinc and nickel), very strong higher binding energy contributions are seen which diminish rapidly with annealing below 300°C.[38-40] In our case, no significant reduction in the higher binding energy signal at 289.1eV is observed until the annealing temperature is raised to 450°C, 100°C higher than the temperature generally employed to decompose the substrate coating and ~200°C over the melting temperature of zinc acetate.[13,41] The resistance of the higher binding energy peak to annealing at 350°C is inconsistent with the behaviour of acetates, as a significant decrease in such signals is expected when acetate salts are annealed at temperatures as low as 250°C, as mentioned above. [39-40] These data therefore suggest that the origin of the signal is primarily due to strongly chemisorbed atmospheric carbonates.

Carbon- C1s

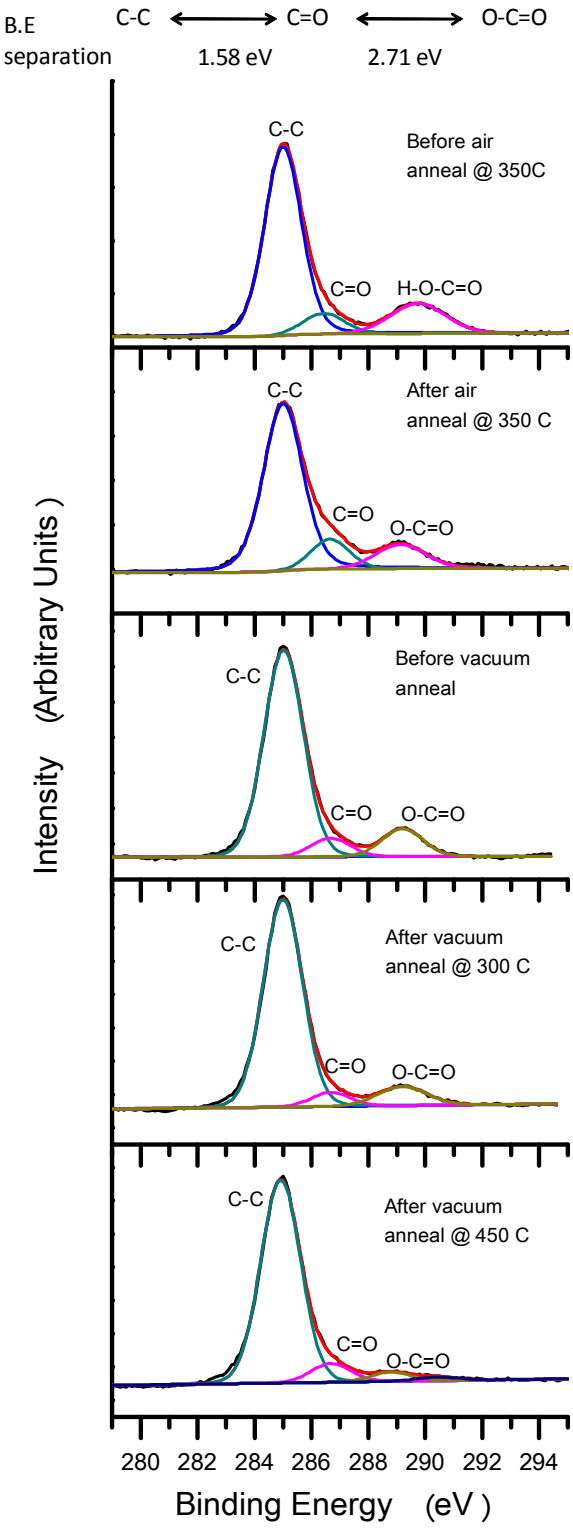
B.E separation
C-C
C=O
O-C=O
1.58 eV
2.71 eV
C-C
Before air anneal @ 350C
C=O
H-O-C=O
C-C
After air anneal @ 350 C
C=O
O-C=O
C-C
Before vacuum anneal
C=O
O-C=O
C-C
After vacuum anneal @ 300 C
C=O
O-C=O
C-C
After vacuum anneal @ 450 C
C=O
O-C=O
Intensity (Arbitrary Units)
280 282 284 286 288 290 292 294
Binding Energy (eV)

Figure 1: XPS Spectra showing carbon region of the spectrum, before and after annealing in air, and before and after annealing under vacuum at 300°C and 450°C.

In the oxygen O1s region of the spectrum, shown in figure 2, the dominant spectral component in both samples prior to annealing is Zn-OH around 532.5 eV[42-43] with a smaller ZnO contribution at 530.5 eV. While the precise origin of the ZnO component prior to annealing is unknown, it may be due to a partial photo-induced decomposition of zinc hydroxide.[44] The strong emission peak at ~536.6 eV associated with zinc acetate observed by other groups[40] was not detected in any samples either before or after annealing, and would be easily resolved in our experiment if it was present. The complete absence of this peak in any of the samples, strongly suggests that the thin film formed at the substrate surface is not due to a residual acetate film and that the chemical pathway proceeds via the zinc hydroxide intermediate. The sample held in air prior to annealing had an additional carbonate component at 532 eV, which was not detected in the sample held in vacuum. However this carbon-derived signal is substantially weaker than the zinc hydroxide component. A small carbon-derived signal at ~533.8 eV is detected in the samples held in vacuum both before and after annealing. After annealing both in air and in vacuum the ZnO peak at 530.5 eV increases substantially while the zinc hydroxide component is attenuated, as shown in figures 2.

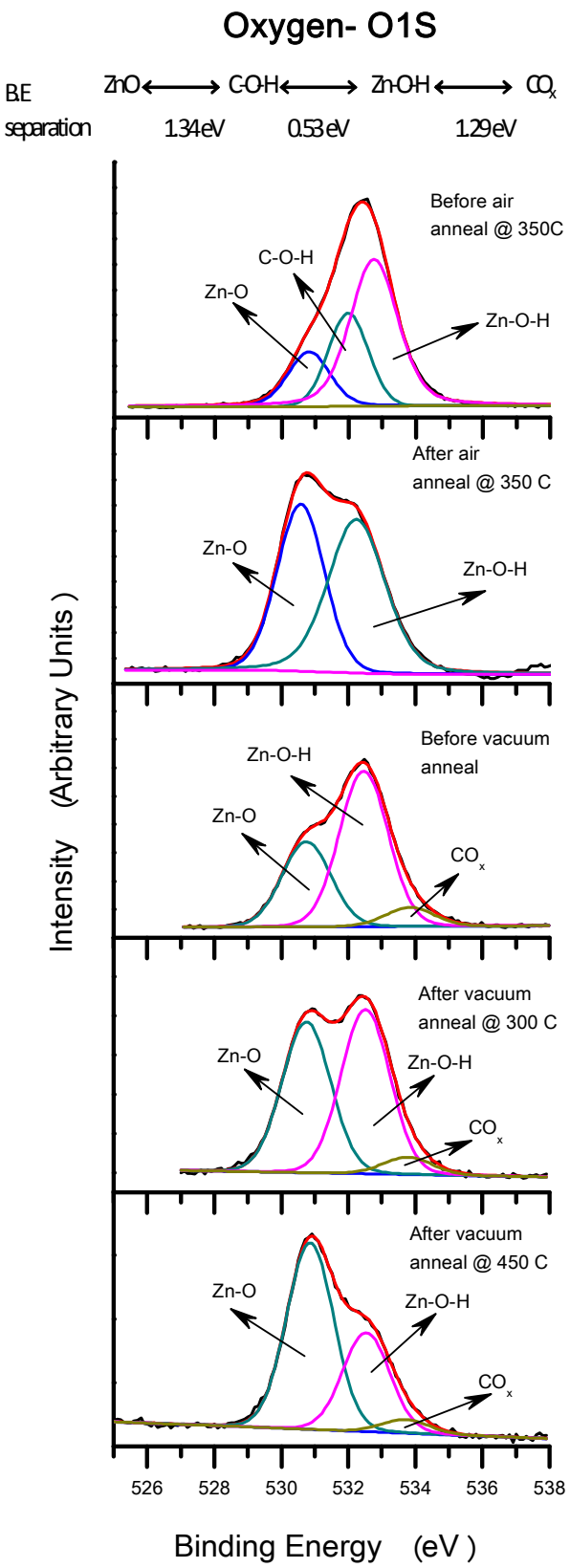
Oxygen- O1S
BE separation
ZnO
C-O-H
Zn-O-H
CO$_x$
1.34eV
0.53eV
1.29eV
Before air anneal @ 350C
C-O-H
Zn-O
Zn-O-H
After air anneal @ 350 C
Zn-O
Zn-O-H
Before vacuum anneal
Zn-O-H
Zn-O
CO$_x$
After vacuum anneal @ 300 C
Zn-O
Zn-O-H
CO$_x$
After vacuum anneal @ 450 C
Zn-O
Zn-O-H
CO$_x$
Intensity (Arbitrary Units)
526
528
530
532
534
536
538
Binding Energy (eV)

Figure 2: XPS Spectra showing oxygen region of the spectrum, before and after annealing in air, and before and after annealing under vacuum at 300°C and 450°C.

Overall the photoemission results indicate that prior to annealing the dominant component of the substrate coating is zinc hydroxide which transforms to ZnO after annealing. As XPS is a surface characterisation technique with a shallow sampling depth, the presence of both oxide and hydroxide species in the XPS spectra is symptomatic of the surface reactivity of ZnO and therefore very difficult to avoid. The smaller quantities of carboxyl/acetate-based compounds do not appear to play a significant role in the formation of the ZnO seed layer. The complete absence of the higher binding energy contribution in the O1S region associated with zinc acetate[40], suggests that it is either completely absent or present in such small quantities as to be beyond the limit of detection of our XPS system. These results are supported by XPS data from the Zn2P3/2 spectral region (data not shown).

The conclusions above concerning the chemical pathway for acetate-derived seed growth are in full agreement with the mechanism proposed by Lee *et. al.*[32], specifically that the diffusion of atmospheric water into the zinc acetate solution leads to the precipitation of zinc hydroxide. From this one can conclude that the controlling factors during acetate-derived seed layer preparation include the relative humidity during drop coating, which provides the driving force for the diffusion of water across the air-fluid interface, and the fluid thickness which must be sufficiently thin to allow the precipitate to reach and deposit on the substrate surface before the solution is washed off.

3.2 Comparison of VPT growth using one-stage and two-stage buffer layers

Following the seed layer preparation, short nanorods were grown on the substrates by two different CBD techniques as described in the experimental section and references.[13, 45] Figure 3 shows plan and cross-sectional views of typical results obtained for these processes, with both techniques yielding aligned nanorod arrays ~300-500nm in length with diameters of ~80-180 nm. The factors affecting chemical bath depositions are not examined in this work as this has been studied extensively elsewhere.

Hereafter layers prepared by drop coating zinc acetate solutions and those prepared by drop coating zinc acetate solutions followed by CBD are referred to as one-stage and two-stage buffer layers respectively.

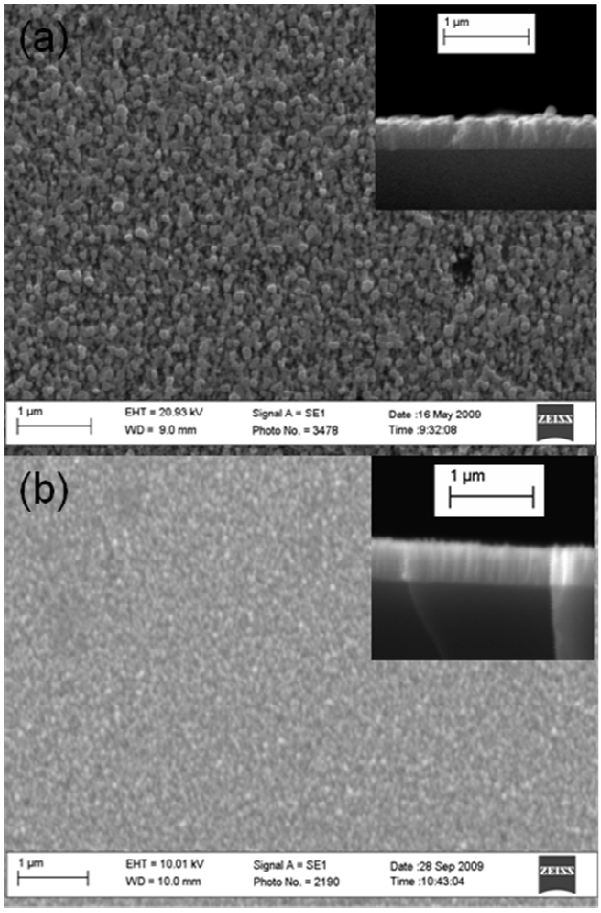

Figure 3: SEM images showing (a) plan view and (insert) cross-sectional view of the nanorod array deposited using the hexamine-based method and (b) plan view and (insert) cross-sectional view of the nanorod array deposited using the NaOH-based method.

After the preparation of one-stage and two-stage buffer layers, VPT growth was performed on both sets of substrates. The VPT technique used during this step differed slightly from many previously reported methods, as no inner tube was used in the furnace and the substrates were placed directly above the ZnO-graphite mix, thereby maintaining the substrate and source powder at the same temperature. Striking differences can be observed between the depositions on each sample set. Figure 4 shows the plan views(a,b), 45° views(c) and cross-sectional views(d) of nanorods deposited on a one-stage buffer layer. Here it can be seen that the bulk of nanorod growth took place at the substrate edges. Dense,

poorly-aligned, nanorod growth extends out form the edge of the substrate. Beyond approximately 300µm from the substrate edge, the density of nanowires rapidly decreases and small clusters / single nanorods appear to nucleate from small separated islands. These nucleation points at the base of the nanorods can be clearly seen in figure 4(d). In the lower density regions the nanorods are straight with the poor alignment with respect to the substrate being caused by the nucleation site misalignment. In the higher density regions the misalignment is a combination of nanorod bending and nucleation site misalignment. The nanorods in both high density and low density regions have an interesting morphology. The bases of the rods have a wide diameter of approximately 2-3 µm. After approximately 7-8 µm the diameters of the rods reduces significantly to 800-900 nm at a specific point, which creates a sharp step along the length of the rod, similar to the stepped rod bases previously reported.[46-47] The total lengths of the rods, including the rod bases, vary substantially from 20 µm up to 50 µm. By increasing the number of drop coats used for the one-stage buffer layer deposition prior to VPT deposition, the density of nanorod growth across the substrate increases.

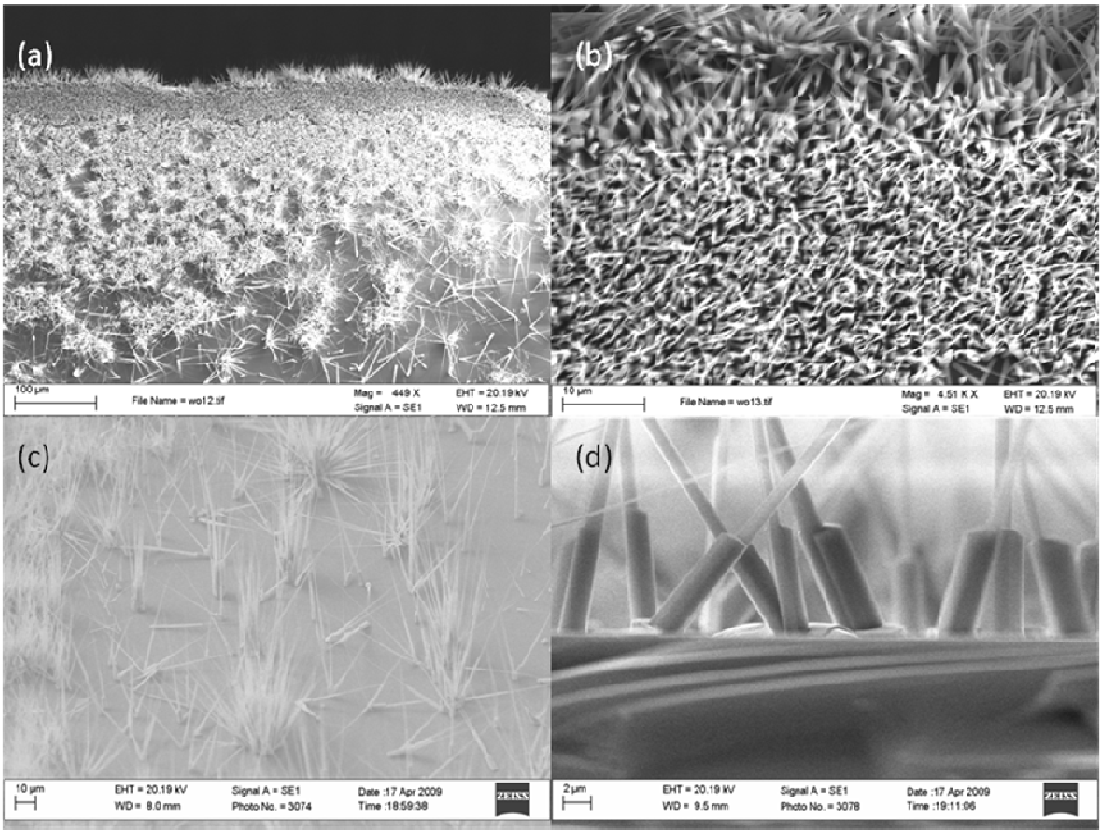

Figure 4 Carbothermal reduction growth on a thin (5 drop coat) one-stage buffer layer at 925°C with a 90sccm argon flow for 1hour (a) Wide plan view of the substrate edge (b) Higher magnification plan view close to the substrate edge (c) 45° view approximately 200µm from the substrate edge (d) 90° view approximately 200µm from the substrate edge.

The SEM images shown in figure 5 are of a substrate that was drop-coated 30 times prior to carbothermal deposition. The entire substrate surface was covered with a dense array of poorly-aligned nanorods, similar to the deposition observed at the edges of thin buffer layered substrates (≤5 drop-coats). The unusual step in rod diameter is not as evident as on the samples grown on thin one-stage buffer layers but some rods do have smaller thinner rods emerging from their tips. As with the thinner (5 drop coat) one-stage buffer layers, the misalignment appears to stem from a combination of nucleation site misalignment and rod bending. There is also some indication of rods coalescing into unified structures at random points along their various growth axes. The diameters of the rods vary substantially from 100 nm to 600nm. A precise measurement of the rod lengths is difficult to determine due to rod bending and coalescence. Despite the increase in substrate coverage with increasing number of drop coats, at the high VPT deposition temperatures the rods grown by VPT on one-stage buffer layers lose their alignment in all samples we have observed.

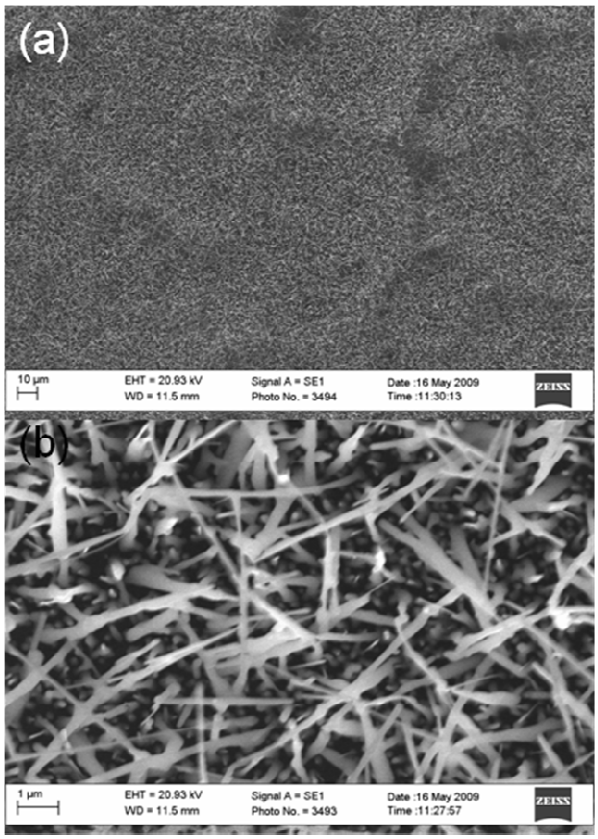

Figure 5**:** SEM images of VPT growth on a thick (30 drop coat) one-stage buffer. (a) Wide plan view (b) Higher magnification plan view close to the centre of the sample

In marked contrast to the nanorod growth on one-stage buffer layer, growth on two- stage buffer layers as shown in figure 6 shows excellent alignment with respect to the substrate. In addition coverage across the substrate was uniform, with a high density of nanorods of uniform length. Nanorod growth on both the hexamine and NaOH-derived two-stage buffer layers showed no significant differences. Samples as large as 4 cm^2 area have been deposited, with a high degree of uniformity in nanorod length and diameter across the entire substrate area, an example of which can be seen in the supporting information (figure S1). As stated in the introduction, nanorods deposited in this manner are of significantly higher quality, as determined by the low temperature PL bound exciton linewidths, than those deposited by CBD techniques. Evidence of this can be seen in the supporting information (figures S2(a) & (b)), where nanorods grown by VPT on two-stage buffer layers have strong and spectrally narrow PL emissions at 18K (~ 3.6 meV full width at half maximum), while nanorods deposited from hexamethyltetramine in

solution have much wider emission linewidths and much lower peak emission intensities (~ 159 meV full width at half maximum and at least an order of magnitude smaller peak intensities).

Variations in nanorod diameter have been observed between samples depending on VPT growth conditions. When the substrate is placed closer to the source powder (~7 mm), using a smaller alumina boat, the nanorod diameter decreases to approximately 80 nm. Using a larger alumina boat where the substrate is further from the source powder leads to an increase in the nanorod diameter. Similar variations in nanorod diameter have also been observed by varying the deposition temperature. At lower temperatures (850°C) thicker nanorods are deposited while at higher temperatures (925°C) thinner nanorods are deposited. These variations in diameter would suggest that the growth process may be sensitive to the Zn vapour concentration. At lower temperatures one would expect the rate of Zn vapour production to be reduced compared to the rate at higher temperatures. When the substrate is placed further above the source powder the volume of space between the source powder and substrate is increased, thereby reducing the concentration of Zn vapour. In both cases an increase in nanorod diameter is observed. To test this theory, VPT growth was performed on a substrate placed close to the source powder (~7 mm). The source powder was compressed into the alumina, reducing the porosity of the material. A firm white crust formed on the upper surface of the source powder after growth where the Zn vapour was unable to escape. Reducing the Zn vapour escaping the powder in this manner leads to a corresponding increase in the nanorod diameter to approximately 220 nm as shown in the supporting information (figure S3). This provisional confirmation of the sensitivity of the nanorod diameter to the Zn vapour concentration also suggests that mixing during preparation and the final porosity of the source powder can lead to variations in the final morphology of the VPT-grown nanorods.

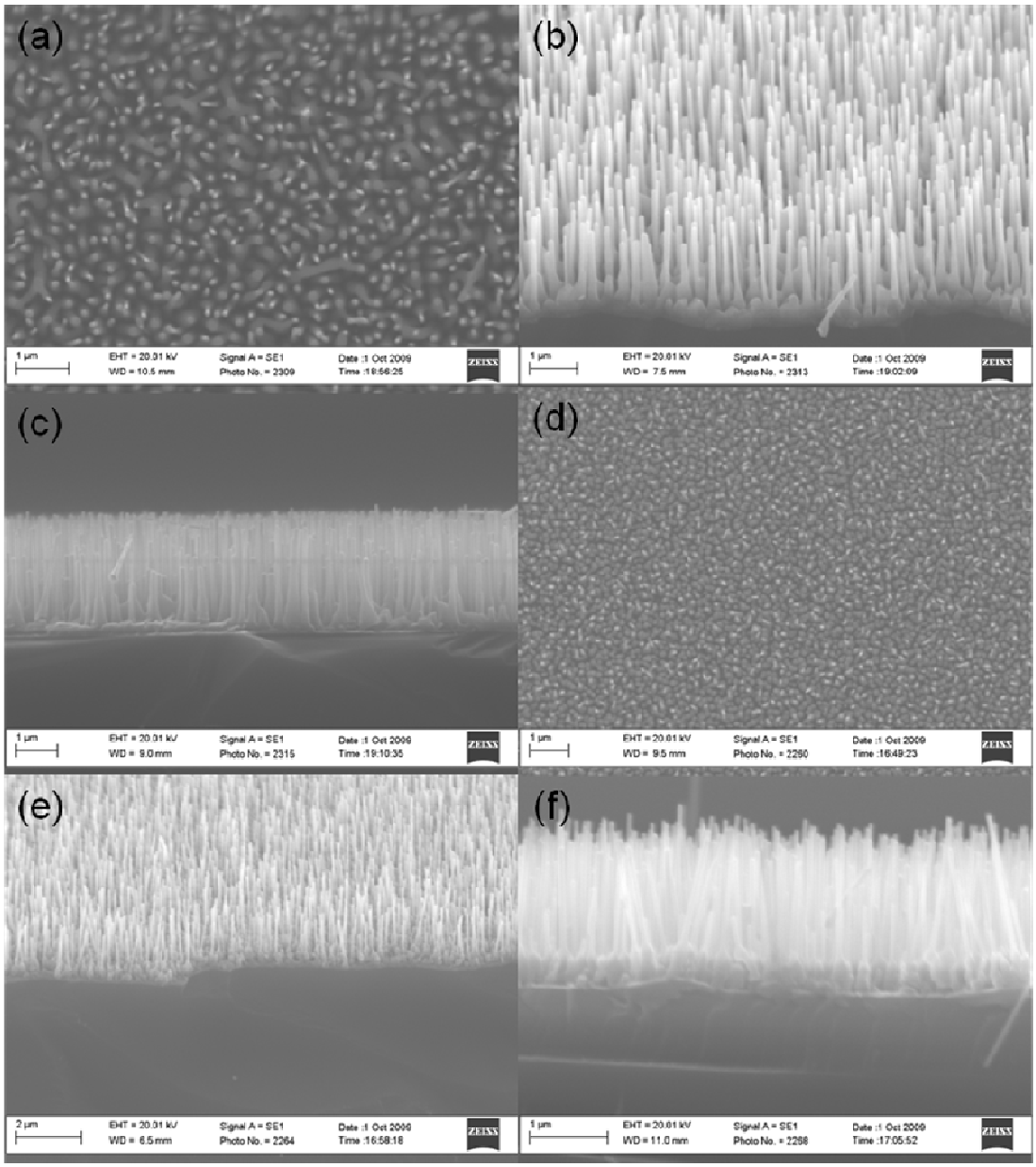

Figure 6: SEM images of VPT growth using two-stage buffer. (a) Plan view (b) 45° view (c) 90° view or nanorod array deposited on hexamine-derived buffer layer. (d) Plan view (e) 45° view (f) 90° view of nanorod array deposited on NaOH-derived buffer layer.

3.2.1 Investigation of one-stage buffer layers

The one-stage buffer layers were further investigated in an attempt to understand why growth was misaligned and only took place at the edges of the substrate during VPT growth, despite there being sufficient nucleation sites for growth to take place across the sample, as demonstrated by CBD growth

runs. Figure 7 shows AFM images of the one-stage buffer layer (5 drop coats) which has been etched on one side with a dilute (1mg/ml) H_2SO_4 solution. The bulk of the substrate is covered with a thin layer of ZnO, composed of millions of small crystallites as shown in figure 7(a). Cross sectional analysis indicate that the crystallites have diameters of 10-20nm and thickness ranging from 2 to 4nm. A substantial variation in the film thickness and composition is observed as the substrate edge is approached. In the region where VPT nanorod growth takes place (figure 7(b)) the film becomes less uniform, being composed of both small crystallites and larger, bulkier crystals, up to 100nm thick. White light profilometry of a sample drop-coated 15 times, as shown in figure 8, clearly demonstrates the variation in thickness across the substrate. A ridge up to 250nm thicker than the bulk of the substrate is observed at the edges of the substrate, where VPT growth takes place.

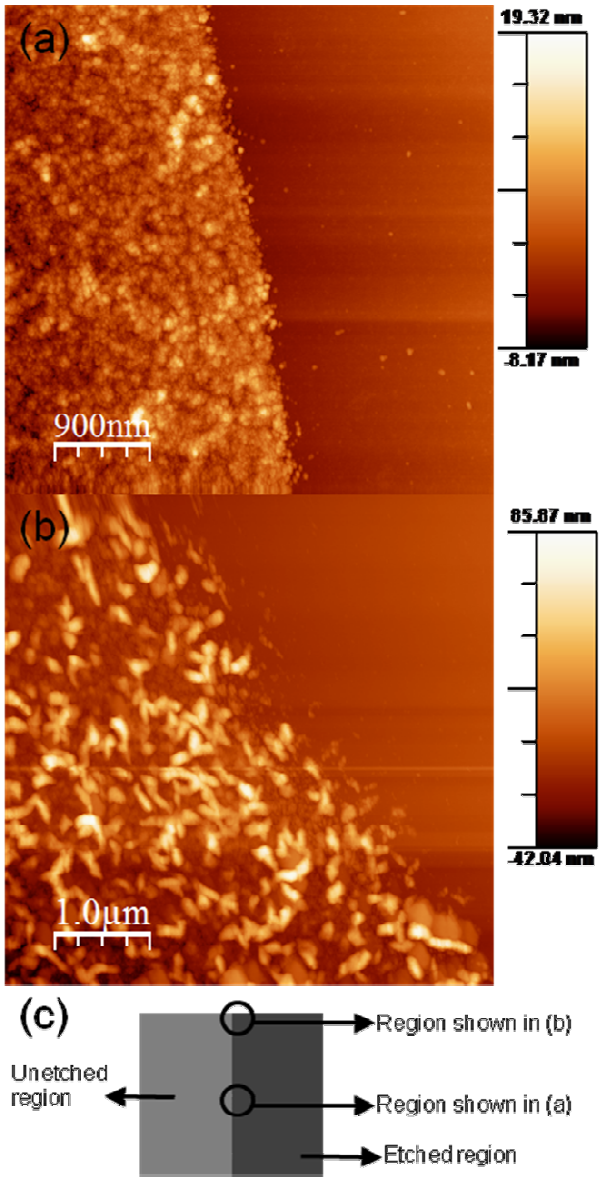

Figure 7: AFM images of (a) one-stage buffer (5 drop coats) layer close to the centre of the substrate (b) one-stage buffer layer close to the edge of the substrate. In both (a) and (b) half of the buffer layer was removed by etching in a dilute H_2SO_4 solution.(c) A schematic representation of the regions analysed in (a) and (b).

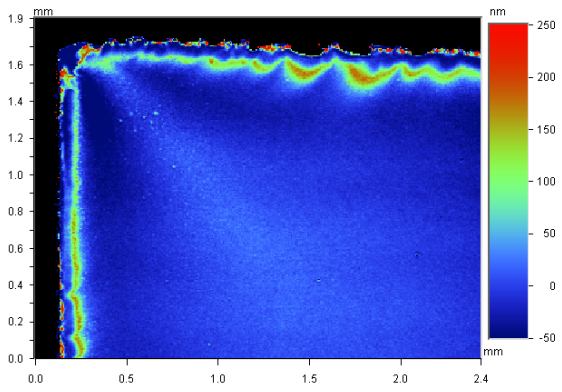

Figure 8: White light surface profile of a substrate with a one-stage buffer layer (15 drop coats)

The one-stage buffer layers were re-analysed after treating them to an identical thermal cycle as the VPT deposition, without the addition of any graphite/ZnO powder. During the heat treatment cycle all reaction parameters, such as argon flow (90 sccm), substrate positioning, and anneal temperature (925°C) and duration were kept the same as during an actual VPT deposition run.

Annealing at a nominal furnace temperature of 925°C has a dramatic effect on the thin one-stage buffer layers, as shown in figure 9. The small individual crystallites are no longer detected and have been replaced by larger structures, reducing the density of seeds dramatically. Similar growth in crystal grain size has been previously reported. It has been observed that annealing ZnO at high temperature causes neighbouring crystals to merge.[48-49] Zhi *et. al.* have suggested this phenomenon is due to defect sites at crystal grain interfaces being favourable sites for crystal coalescence. At the surface of each crystal there are many defects such as dangling bonds, which increase chemical potential, leading to a higher reactivity at the surface.[48] At the substrate edges, the larger crystals also undergo grain growth, leading to random ridged structures. While studying residual stress relaxation in ZnO thin films Ozen *et. al.* have observed strong structural changes in thin ZnO film annealed at high temperature, including stress induced diffusive crystal growth.[50] The thermal energy provided by the annealing promotes pore growth and mass transport though ZnO films accompanying stress relief. In addition, other effects such as plastic deformations, film cracking and delamination were observed.[50] The thin one-stage buffer

layers, composed of random crystallites are likely to have a substantial number of pores in the film. Upon annealing a combination of effects may be leading to the failure of the film including pore coalescence causing film cracking and delamination, diffusive crystal growth and crystal grain growth. The edges of the substrates, being thicker and more robust, are less likely to undergo deformation leading to delamination but the grain growth with annealing destroys the seed alignment.

Two-stage buffer layers, being substantially thicker, undergo fewer deformations. The CBD nanorods in the two-stage buffer layers are significantly longer/thicker than the small thin crystallites in the one-stage buffer layers. During high temperature deposition the hexagonal cylinder nanorods are spatially confined by the presence of neighbouring nanorods, limiting the amount of thermally induced deformations and preserving c-axis alignment. Both AFM and SEM (available in the supporting information, figures S4 & S5) analysis of two-stage buffer layers annealed at 925°C show signs of crystal grain growth, but there are no apparent signs of diffusive crystal growth, crack formation or delamination. At present TEM investigations of the one and two-stage buffer layers are underway, to determine the structure of the nanorods at the substrate interface and to shed further information on the crystal growth process.

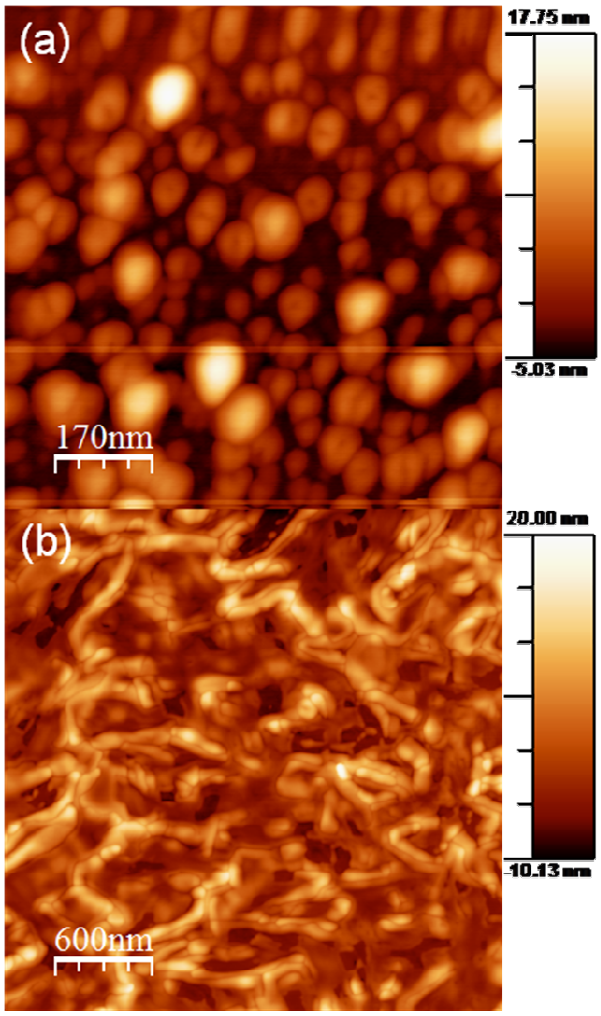

Figure 9: AFM images of (a) one-stage buffer layer close to the centre of the substrate which has been annealed at 925°C using identical parameters as the VPT growth (b) one-stage buffer layer close to the edge of the substrate which has been annealed at 925°C using identical parameters as the VPT growth.

4. Conclusions

XPS analysis of buffers layers generated from drop coating zinc acetate solutions have revealed that the intermediate surface coating is comprised mainly of zinc hydroxide, with a negligible contribution from acetate/carbonate species. Our results are fully consistent with mechanism put forward by Lee *et. al.*, whereby atmospheric water diffuses into the alcohol solution leading to a precipitate of insoluble zinc hydroxide crystals, which are subsequently decomposed during annealing to yield an aligned ZnO buffer layer. While these one-stage buffer layers are suitably robust to withstand CBD growth, high

temperature VPT growth results in poor substrate coverage and/or loss of nanorod alignment. AFM analysis indicates that while the acetate-derived one-stage buffer layers are uniform across most of the substrate, a thicker, more robust, ridge is formed at the substrate edges. During higher temperature VPT deposition the one-stage buffer layer undergoes substantial morphological changes, leading to a severe reduction in the number of available nucleation sites at the sample centre, resulting in the bulk of nanorod growth taking place on the thicker ridges found at the substrates edges, and a loss of alignment of the VPT-grown nanorods. A catalyst-free technique to grow aligned nanorods has been demonstrated using two-stage buffer layers, using acetate-derived seeds and low temperature CBD-grown short nanorods, combined with high temperature VPT nanorod deposition, which results in well-aligned nanorod arrays with excellent, uniform, substrate coverage over large areas. This method offers distinct advantages over other techniques in that it is, reproducible, compatible with a variety of substrate types and potentially scalable for industrial applications.

Acknowledgements

DB, GH and EMCG acknowledge a Science Foundation Ireland Strategic Research Cluster grant entitled “Functional Oxides and Related Materials for Electronics” (FORME). DB and EMCG gratefully acknowledge helpful discussions with Prof. Martyn Pemble (Tyndall National Institute, Ireland - PI of FORME cluster) on the chemical reactions involved in the seeding mechanism. DB would like to thank Dr. Tony Cafolla and Dr. Barry O’Connell for assistance and support with AFM and white light profilometry measurements, respectively.

Supporting Information Available

S1) SEM images of VPT growth on two-stage buffer layers

S2) Low temperature PL spectrum of ZnO nanorods deposited on one-stage and two stage buffer layers

S3) SEM images of VPT growth on two-stage buffer layer using a smaller alumina boat and compressed source powder during CTR step

S4) AFM images of unannealed HMT-derived two-stage buffer layer and HMT-derived two-stage buffer layer annealed at 925°C

S5) SEM images of of unannealed HMT-derived two-stage buffer layer and of HMT-derived two-stage buffer layer annealed at 925°C

This information is available free of charge via the Internet at http://pubs.acs.org/.

References

(1) Reynolds, D. C.; Look, D. C.; Jogai, B.; Litton, C. W.; Collins, T. C.; Harsch, W.; Cantwell, G. *Phys. Rev. B.* **1998,** *58* (19) 13276-13276

(2) Ozgur, U.; Alivov, Y. I.; Liu, C.; Teke, A.; Reshchikov, M. A.; Dogan, S.; Avrutin, V.; Cho, S. J.; Morkoc, H. *J. Appl. Phys.* **2005,** *98* 041301

(3) Lee, C. J.; Lee, T. J.; Lyu, S. C.; Zhang, Y.; Ruh, H.; Lee, H. J. *Appl. Phys. Lett.* **2002,** *81* (19) 3648-3650

(4) Huang, M. H.; Mao, S.; Feick, H.; Yan, H. Q.; Wu, Y. Y.; Kind, H.; Weber, E.; Russo, R.; Yang, P. D. *Science* **2001,** *292* (5523) 1897-1899

(5) Nanto, H.; Minami, T.; Takata, S. *J. Appl. Phys.* **1986,** *60* (2) 482-484

(6) Wang, J. X.; Sun, X. W.; Yang, Y.; Huang, H.; Lee, Y. C.; Tan, O. K.; Vayssieres, L. *Nanotechnology* **2006,** *17* (19) 4995-4998

(7) Ueda, K.; Muraoka, Y.; Tabata, H.; Kawai, T. *Appl. Phys. Lett.* **2001,** *78* (4) 512-514

(8) Wang, Z. L.; Song, J. H. *Science* **2006,** *312* (5771) 242-246

(9) Li, Z.; Yang, R. S.; Yu, M.; Bai, F.; Li, C.; Wang, Z. L. *J. Phys. Chem. C* **2008,** *112* (51) 20114-20117

(10) Bao, D. H.; Gu, H. S.; Kuang, A. X. *Thin Solid Films* **1998,** *312* (1-2) 37-39

(11) Grabowska, J.; Meaney, A.; Nanda, K. K.; Mosnier, J. P.; Henry, M. O.; Duclere, J. R.; Mcglynn, E. *Phys. Rev. B* **2005,** *71* 115439

(12) Law, M.; Greene, L. E.; Johnson, J. C.; Saykally, R.; Yang, P. D. *Nature Materials* **2005,** *4* (6) 455-459

(13) Greene, L. E.; Law, M.; Tan, D. H.; Montano, M.; Goldberger, J.; Somorjai, G.; Yang, P. D. *Nano Lett.* **2005,** *5* (7) 1231-1236

(14) Chen, Y. X.; Zhao, X. Q.; Sha, B.; Chen, J. H. *Mater. Lett.* **2008,** *62* (15) 2369-2371

(15) Kong, X. Y.; Wang, Z. L. *Nano Lett.* **2003,** *3* (12) 1625-1631

(16) Wang, Y. F.; Chen, X. L.; Zhang, J. H.; Sun, Z. Q.; Li, Y. F.; Zhang, K.; Yang, B. *Colloids Surf., A* **2008,** *329* (3) 184-189

(17) Jo, S. H.; Lao, J. Y.; Ren, Z. F.; Farrer, R. A.; Baldacchini, T.; Fourkas, J. T. *Appl. Phys. Lett.* **2003,** *83* (23) 4821-4823

(18) Xu, H. Y.; Wang, H.; Zhang, Y. C.; He, W. L.; Zhu, M. K.; Wang, B.; Yan, H. *Ceram. Int.* **2004,** *30* (1) 93-97

(19) Govender, K.; Boyle, D. S.; Kenway, P. B.; O'brien, P. *J. Mater. Chem.* **2004,** *14* (16) 2575-2591

(20) Grabowska, J.; Nanda, K. K.; Mcglynn, E.; Mosnier, J. P.; Henry, M. O. *Surf. Coat. Tech.* **2005,** *200* (1-4) 1093-1096

(21) Park, D. J.; Kim, D. C.; Lee, J. Y.; Cho, H. K. *Nanotechnology* **2006,** *17* (20) 5238-5243

(22) Ashfold, M. N. R.; Doherty, R. P.; Ndifor-Angwafor, N. G.; Riley, D. J.; Sun, Y. *Thin Solid Films* **2007,** *515* (24) 8679-8683

(23) Greene, L. E.; Yuhas, B. D.; Law, M.; Zitoun, D.; Yang, P. D. *Inorganic Chemistry* **2006,** *45* (19) 7535-7543

(24) Greene, L. E.; Law, M.; Goldberger, J.; Kim, F.; Johnson, J. C.; Zhang, Y. F.; Saykally, R. J.; Yang, P. D. *Angew Chem Int Edit* **2003,** *42* (26) 3031-3034

(25) Zhao, Q. X.; Yang, L. L.; Willander, M.; Sernelius, B. E.; Holtz, P. O. *J. Appl. Phys.* **2008,** *104* (7) 073526

(26) Kumar, R. T. R.; McGlynn, E.; Biswas, M.; Saunders, R.; Trolliard, G.; Soulestin, B.; Duclere, J. R.; Mosnier, J. P.; Henry, M. O. *J. Appl. Phys.* **2008,** *104* (8) 084309-084311

(27) Zhou, Y.; Wu, W. B.; Hu, G. D.; Wu, H. T.; Cui, S. G. *Mater. Res. Bull.* **2008,** *43* (8-9) 2113-2118

(28) Li, C.; Fang, G. J.; Li, J.; Ai, L.; Dong, B. Z.; Zhao, X. Z. *J. Phys. Chem. C* **2008,** *112* (4) 990-995

(29) Li, C.; Fang, G.; Fu, Q.; Su, F.; Li, G.; Wu, X.; Zhao, X. *J. Cryst. Growth* **2006,** *292* (1) 19-25

(30) Kang, D.-S.; Han, S. K.; Kim, J.-H.; Yang, S. M.; Kim, J. G.; Hong, S.-K.; Kim, D.; Kim, H.; Song, J.-H. *J. Vac. Sci. Technol. B* **2009,** 27 (3) 1667-1672

(31) Byrne, D.; Mcglynn, E.; Henry, M. O.; Kumar, K.; Hughes, G. *Thin Solid Films In Press, Corrected Proof*

(32) Lee, Y. J.; Sounart, T. L.; Scrymgeour, D. A.; Voigt, J. A.; Hsu, J. W. P. *J. Cryst. Growth* **2007,** *304* (1) 80-85

(33) Moulder, J. F.; Stickle, W. F.; Sobol, P. E.; Bomben, K. D., eds. *Handbook of X-Ray Photoelectron Spectroscopy* 1st ed., ed. J. Chastain. 1992, Perkin-Elmer Corporation: Eden Prairie, Mn.

(34) Wang, J.; Hokkanen, B.; Burghaus, U. *Surf. Sci.* **2005,** *577* (2-3) 158-166

(35) Gutierrez-Sosa, A.; Evans, T. M.; Parker, S. C.; Campbell, C. T.; Thornton, G. *Surf. Sci.* **2002,** *497* (1-3) 239-246

(36) Moller, P. J.; Komolov, S. A.; Lazneva, E. F.; Pedersen, E. H. *Surf. Sci.* **1995,** *323* (1-2) 102-108

(37) Saw, K. G.; Ibrahim, K.; Lim, Y. T.; Chai, M. K. *Thin Solid Films* **2007,** *515* (5) 2879-2884

(38) Mar, G. L.; Timbrell, P. Y.; Lamb, R. N. *Chem. Mater.* **1995,** *7* (10) 1890-1896

(39) Jesus, J. C. D.; Gonzalez, I.; Quevedo, A.; Puerta, T. *J. Mol. Catal. A: Chem.* **2005,** *228* (1-2) 283-291

(40) Mar, L. G.; Timbrell, P. Y.; Lamb, R. N. *Thin Solid Films* **1993,** *223* (2) 341-347

(41) Zhao, X. Y.; Zheng, B. C.; Li, C. Z.; Gu, H. C. *Powder. Technol.* **1998,** *100* (1) 20-23

(42) Hsieh, P. T.; Chen, Y. C.; Kao, K. S.; Wang, C. M. *Appl. Phys. A-Mater.* **2008,** *90* (2) 317-321

(43) Ramgir, N. S.; Late, D. J.; Bhise, A. B.; More, M. A.; Mulla, I. S.; Joag, D. S.; Vijayamohanan, K. *J. Phys. Chem. B* **2006,** *110* (37) 18236-18242

(44) Hu, X. L.; Masuda, Y.; Ohji, T.; Kato, K. *Langmuir* **2008,** *24* (14) 7614-7617

(45) Peterson, R. B.; Fields, C. L.; Gregg, B. A. *Langmuir* **2004,** *20* (12) 5114-5118

(46) Kumar, R. T. R.; McGlynn, E.; McLoughlin, C.; Chakrabarti, S.; Smith, R. C.; Carey, J. D.; Mosnier, J. P.; Henry, M. O. *Nanotechnology* **2007,** *18* 215704

(47) Yang, L. W.; Wu, X. L.; Xiong, Y.; Yang, Y. M.; Huang, G. S.; Chu, P. K.; Siu, G. G. *Journal of Crystal Growth* **2005,** *283* (3-4) 332-338

(48) Zhi, Z. Z.; Liu, Y. C.; Li, B. S.; Zhang, X. T.; Lu, Y. M.; Shen, D. Z.; Fan, X. W. *J. Phys. D. Appl. Phys.* **2003,** *36* (6) 719-722

(49) Hong, R. J.; Huang, J. B.; He, H. B.; Fan, Z. X.; Shao, J. D. *Appl. Surf. Sci.* **2005,** *242* (3-4) 346-352

(50) Ozena, I.; Gulgunb, M. A. *Adv. Sci. Technol.* **2006,** *45* 1316-1321